JOINT INSTITUTE FOR AERONAUTICS AND ACOUSTICS

National Aeronautics and
Space Administration

Ames Research Center

JIAA TR - 94

Stanford University

ANALYSIS OF INTERNAL ABLATION FOR THE THERMAL CONTROL OF AEROSPACE VEHICLES

By

Jose A. Camberos and Leonard Roberts

Stanford University
Department of Aeronautics and Astronautics
Stanford, CA 94305

AUGUST 1989

Abstract

In this report, a new method of thermal protection for transatmospheric vehicles is introduced. The method involves the combination of radiation, ablation and transpiration cooling. By placing an ablating material behind a fixed-shape, porous outer shield, the effectiveness of transpiration cooling is made possible while retaining the simplicity of a passive mechanism. A simplified one-dimensional approach is used to derive the governing equations. Reduction of these equations to non-dimensional form yields two parameters which characterize the thermal protection effectiveness of the shield and ablator combination for a given trajectory.

The non-dimensional equations are solved numerically for a sample trajectory corresponding to glide re-entry. Four typical ablators are tested and compared with results obtained by using the thermal properties of water. For the present level of analysis, the numerical computations adequately support the analytical model.

Nomenclature

A	dimensionless ablation parameter defined in text
c	heat capacity (specific heat, constant pressure) J/kg/K
F	dimensionless heating rate function
G	dimensionless total heat input function
H_o	total (stagnation point) enthalpy of free stream, J/kg
HC	threshold enthalpy of ablating material, J/kg
HL, L	enthalpy of ablation, J/kg
m	mass per unit area, kg/m^2
q_o	stagnation point convective heating rate, W/m^2
q_r	re-radiation heating rate, W/m^2
Q	total heat input (heating rate integrated over time), J/m^2
R	dimensionless radiation parameter
t	time, s
T	temperature, K
V	dimensionless mass flux
x,y,z	cartesian coordinate system

Greek Symbols

α absorptivity coefficient

β parameter, used in reduced form of equations in text

δ dimensionless integral thermal thickness

ϵ emissivity

η transpiration coefficient

ρ density (kg/m^2)

σ Stefan-Bolzman constant = $5.67 \times 10^{-3} W/m^2 K^4$

k conductivity, $W/m/K$

Subscripts

a ablator property at time of ablation

b solid ablation material, virgin state

o stagnation point value

r radiative

s ablation surface prior to ablation

w shield wall

∞ free-stream property

Superscripts

* critical, maximum value

List of Figures

1.0 Introduction

Radiating ablation materials have seen extensive use for the protection of aerospace vehicles over the past thirty years, notable examples being the ICBM nose cones and the manned spacecraft Mercury, Gemini and Apollo. These materials have successfully served the purpose of thermal protection but have distinct disadvantages for reusable vehicles, particularly those for which the gometry determines the aerodynamic performance. The use of such ablation materials in regions of localized high heating rates, such as the nose or leading edge of the wing leads to significant changes in shape over critical aerodynamic surfaces with consequent adverse effects on performance characteristics.

In order to overcome such disadvantages while retaining the inherent passive simplicity of the radiating ablation approach, a new concept is studied in this paper: an internal ablator protected by a fixed-shape porous outer radiating structure. This approach permits leading edges and other regions of intense localized heating to be radiatively cooled over most of the flight trajectory. When excessive heating occurs however, ablation results and causes the transpiration of gaseous products through the outer radiating structure, thus controlling its temperature. The introduction of ablation products into the external boundary layer reduces the net heat flux to the outer surface thus providing a passive thermal protection mechanism.

This approach to thermal protection depends on the judicious choice of thermal properties of the outer structure and the internal ablator. The analysis given in this paper provides the thermal parameters which assure that the external surface temperature of the radiating structure will not exceed specified limits during the heating period while avoiding excessive mass loss from the internal ablation material. Approximate methods of analysis are used to identify the important thermal parameters in dimensionless form which may be used for the selection of material properties.

1.1 Description of the Concept

The radiation/ablation concept considered here consists of a porous fixed-shape outer structure, the temperature of which is limited to a value T^* (see Fig. 1.1). Behind this outer structure is placed an ablator of sufficient thickness such that its back surface temperature T_b remains constant while its front surface when heated will ablate at a characteristic temperature T_a. During ablation gaseous products transpire through the fixed outer structure into the external boundary layer thereby providing the means for reducing the heat transfer rate to the outer surface. Heat transfer between the outer structure and the ablation surface is by radiation across the gap, thermal conduction in the gaseous products within the gap is ignored. A planar geometry is considered corresponding to the region near the stagnation point of the vehicle nose or near the stagnation line of the wing. Extension of the concept to other geometries should be straightforward.

2.0 Concept Analysis

In the present analysis it is assumed that the outer structure is of high thermal conductivity and attains a uniform temperature $T_w(t)$ which must be limited throughout the flight to a value less than some maximum value T^*. This structure is perforated to allow for the transpiration of ablation products into the boundary layer which thereby provide a reduction in the heating rate. The outer structure radiates outward at a rate $q_r(t)$ and also radiates inward at a rate $\alpha q_r(t)$ to the ablation surface, where α is the absorption coefficient of the ablation material.

It is assumed that the ablation material has a surface temperature $T_s(t)$ which increases to a fixed value T_a when ablation occurs. The ablation material is considered sufficiently thick to permit its back surface temperature to maintain a constant value T_b.

Thermal Balance Equations

In the absence of ablation the thermal balance at the outer surface can be written

$$(1+\alpha)q_r(t) = q_o(t) \tag{2.1}$$

where $q_r(t) = \sigma\epsilon T_w^4$ and $q_o(t)$ is the convective heating rate for the given trajectory. When ablation occurs, however, transpiration through the outer structure into the boundary layer flow causes a reduction in the heating rate, which can be expressed in simplified form as

$$(1+\alpha)q_r(t) = q_o - \eta H_o \frac{dm}{dt} \tag{2.2}$$

In equation (2.2) H_o is the total stream enthalpy, η is an efficiency factor which depends on the state of the boundary layer (laminar or turbulent) and on the molecular weight of the ablation products, and dm/dt is the rate of mass transpiration. The factor η lies in the range $1/3 < \eta < 2/3$ for typical ablation materials. The quantities $q_r(t)$ and dm/dt are in general unknown and must be determined by considering the heat radiated to the ablation surface and the conduction of heat within the ablation material.

It is convenient to define a thermal integral thickness $\theta(t)$ within the ablation material such that the heat content of the material is $\rho c(T_s - T_b)\theta$ where $(T_s - T_b)$ is the temperature rise at the surface[1-3]. Thus

$$\theta = \int_{-\infty}^{o} \frac{T - T_b}{T_s - T_b} dz \tag{2.3}$$

The overall heat balance, in differential form, for the ablation material, is then

$$\alpha q_r(t) = [c_b(T_a - T_b) + L]\frac{dm}{dt} + \rho_b c_b \frac{d}{dt}[(T_s - T_b)\theta] \tag{2.4}$$

where L is the enthalpy of ablation (vaporization) and $c_b(T_a - T_b)$ is the threshold enthalpy rise prior to vaporization. An additional equation representing the heating rate boundary condition at the ablation surface is written

$$\alpha q_r(t) = L\frac{dm}{dt} + k_b\left(\frac{dT}{dz}\right)_{z=0} \tag{2.5}$$

Equation (2.5) represents a heat transfer rate balance. Since the ablator is considered to have thickness much larger than θ the approximation

$$k_b\left(\frac{dT}{dz}\right)_0 = \frac{k_b(T_s - T_b)}{\theta}$$

can be made, with the result that equation (2.5) is written

$$\alpha q_r(t) = L\frac{dm}{dt} + \frac{k_b(T_s - T_b)}{\theta} \tag{2.5a}$$

Finally the unknown quantity $q_r(t)$ can be eliminated from equations (2.4) and (2.5a) through the use of equation (2.2) to give

$$\left(\frac{\alpha}{1+\alpha}\right) q_o(t) = \left[c_b(T_a - T_b) + L + \left(\frac{\alpha}{1+\alpha}\right)\eta H_o\right]\frac{dm}{dt} + \rho_b c_b \frac{d}{dt}\left[(T_s - T_b)\theta\right] \tag{2.6}$$

and

$$\left(\frac{\alpha}{1+\alpha}\right) q_o(t) = \left[L + \left(\frac{\alpha}{1+\alpha}\right)\eta H_o\right]\frac{dm}{dt} + \frac{k_b(T_s - T_b)}{\theta} \tag{2.7}$$

where $q_o(t)$ is the known heating rate that would occur at the outer surface in the absence of ablation and $H_o(t)$ is the total stream enthalpy, both determined from the vehicle trajectory.

Equations (2.6) and (2.7) must be solved either for T_s and θ during periods of non-ablation when $dm/dt = 0$ and for dm/dt and θ during periods of ablation, when $T_s = T_a$.

2.1 Pre-Ablation Heating

During the pre-ablation heating period, $dm/dt = 0$ and equation (2.6) may be integrated to give

$$\left(\frac{\alpha}{1+\alpha}\right) Q_o(t) = \rho_b c_b (T_s - T_b)\theta \tag{2.8}$$

while equation (2.7) reduces to

$$\left(\frac{\alpha}{1+\alpha}\right) q_o(t) = \frac{k_b(T_s - T_b)}{\theta} \tag{2.9}$$

where the total heat input is

$$Q_o(t) = \int_o^t q_o(\zeta) d\zeta$$

Equations (2.8) and (2.9) give the solution

$$(T_s - T_b) = \left(\frac{\alpha}{1+\alpha}\right) \left[\frac{Q_o(t) q_o(t)}{\rho_b c_b k_b}\right]^{\frac{1}{2}} \tag{2.10}$$

and

$$\theta = \left[\frac{Q_o(t) k_b}{q_o(t) \rho_b c_b}\right]^{\frac{1}{2}} \tag{2.11}$$

giving the temperature at the ablator surface and the heat penetration thickness θ. From equation (2.10) the time t_a at which the surface temperature reaches the value T_a is given

implicity by

$$Q_o(t_a)q_o(t_a) = Q_a q_a = \left(\frac{\alpha}{1+\alpha}\right)^2 \rho_b c_b k_b (T_a - T_b)^2 \tag{2.12}$$

and the thermal thickness at this time is $\theta_a = [Q_a k_b / q_a \rho_b c_b]^{\frac{1}{2}}$. Prior to ablation, the surface temperature of the outer structure T_w is given by equation (2.1)

$$\sigma \epsilon T_w^4 = q_r(t) = \frac{q_o(t)}{1+\alpha}$$

or

$$T_w(t) = \left[\frac{q_o(t)}{(1+\alpha)\sigma\epsilon}\right]^{\frac{1}{4}} \tag{2.13}$$

If the maximum outer surface temperature permitted is T^* (corresponding to a heating rate $q_r^* = \sigma \epsilon T^{*4}$) then the time t_a when ablation occurs must satisfy the implicit condition

$$\frac{q_o(t_a)}{(1+\alpha)q_r^*} \leq 1 \tag{2.14}$$

This must be achieved through proper choice of the ablation material properties α, ρ_b, k_b, and T_a as seen from equation (2.12)

2.2 Ablation Heating

During the period of ablation, for which $T_s = T_a$, equations (2.6) and (2.7) become

$$\left(\frac{\alpha}{1+\alpha}\right) q_o(t) = \left[c_b(T_a - T_b) + L + \left(\frac{\alpha}{1+\alpha}\right)\eta H_o\right] \frac{dm}{dt} + \rho_b c_b (T_a - T_b) \frac{d\theta}{dt} \tag{2.15}$$

and

$$\left(\frac{\alpha}{1+\alpha}\right) q_o(t) = \left[L + \left(\frac{\alpha}{1+\alpha}\right)\eta H_o\right]\frac{dm}{dt} + \frac{k_b(T_a - T_b)}{\theta} \tag{2.16}$$

which may be solved for dm/dt and θ. These equations are solved in dimensionless form in Appendix A and approximate analytic solutions are given under the assumption that the enthalpy ratio:

$$\frac{c_p(T_a - T_b)}{\left[c_p(T_a - T_b) + \left(\frac{\alpha}{1+\alpha}\right)\eta H_o\right]} << 1 \tag{2.17}$$

In view of the large value of H_o compared with all other terms in (2.17) this assumption is generally valid.

The approximate solution is written:

$$\theta/\theta_a = [1 + 2\beta_a(t/t_a - 1)]^{\frac{1}{2}} \tag{2.18}$$

and from 2.15

$$\frac{dm}{dt} = \left(\frac{\alpha}{1+\alpha}\right)\frac{q_o(t)}{c_b(T_a - T_b) + L + \left(\frac{\alpha}{1+\alpha}\right)\eta H_o}\left[1 - \frac{q_a}{q_o[1 + 2\beta_a(t/t_a - 1)]^{\frac{1}{2}}}\right] \tag{2.19}$$

where $\beta_a = q_a t_a/Q_a$. The approximate solutions given by (2.18) and (2.19) are valid only as long as the inequality (2.17) holds.

During ablation the temperature of the outer structure is found from

$$\left(\frac{T_w}{T^*}\right)^4 = \frac{q_r}{q_r^*}$$

where q_r is given by equation (2.5a) with θ and dm/dt determined from equations (2.15) and (2.16) respectively. These simplified analytical solutions are presented for the purpose of deriving the relation (2.21) below. The result is written

$$\left(\frac{T_w}{T^*}\right)^4 = \frac{q_a}{(1+\alpha)q_r^*}\left[\frac{\theta_a}{\theta} + \left(\frac{q_o}{q_a} - \frac{\theta_a}{\theta}\right)\cdot\frac{L}{L + \left(\frac{\alpha}{1+\alpha}\right)\eta H_o}\right] \tag{2.20}$$

The solution θ/θ_a is derived in Appendix A, and the approximate solution is given by equation (2.18). In order to assure that $T_w/T^* < 1$ during ablation the latent heat of ablation, L, must be such as to allow the release of an adequate amount of ablation products to cool the outer structure. Equation (2.20) gives $T_w/T^* < 1$ if

$$\frac{q_a}{(1+\alpha)q_r^*}\left[\frac{\theta_a}{\theta} + \left(\frac{q_o}{q_a} - \frac{\theta_a}{\theta}\right)\cdot\frac{L}{[L + (\frac{\alpha}{1+\alpha})\eta H_o]}\right] \leq 1$$

or, after rearrangement of terms:

$$\frac{1}{L} > \left\{\frac{[q_o/q_a - (1+\alpha)q_r^*/q_a]}{[(1+\alpha)q_r^*/q_a - \theta_a/\theta]\cdot[(\frac{\alpha}{1+\alpha})\eta H_o]}\right\}_{\max} \tag{2.21}$$

Thus, the ablation material must satisfy the inequality (2.21) to maintain the shield temperature at or below the required maximum.

2.3 Post-Ablation Heating

From equation (2.16) it can be seen that ablation ceases ($dm/dt = 0$) when

$$\left(\frac{\alpha}{1+\alpha}\right)q_o(t_e) = \frac{k_b(T_a - T_b)}{\theta(t_e)} \tag{2.22}$$

So that $t = t_e$ satisfies the relation $q_e/q_a = \theta_a/\theta_e$ where $q_e = q_o(t_e)$ and $\theta_e = \theta(t_e)$.

For $t = t_e$, equations (2.6) and (2.7) with $dm/dt = 0$ are again used to determine θ and $T_s - T_b$. Equation (2.6) is integrated to give

$$\left(\frac{\alpha}{1+\alpha}\right)\int_{t_e}^{t} q_o(\zeta)d\zeta = \rho_b c_b(T_s - T_b)\theta - \rho_b c_b(T_a - T_b)\theta_e \tag{2.23}$$

and

$$\left(\frac{\alpha}{1+\alpha}\right) q_o = \frac{k_b(T_s - T_b)}{\theta} \tag{2.24}$$

where $q_o(t), t_e, q_e, T_a$ and T_b are all known. Eliminating θ gives

$$\rho_b c_b k_b(T_s - T_b)^2 = \left[\left(\frac{\alpha}{1+\alpha}\right)(Q_o - Q_e) + \rho_b c_b(T_a - T_b)\theta_e\right]\left(\frac{\alpha}{1+\alpha}\right) q_o \tag{2.25}$$

where the change in total heat input is given by integral

$$\int_{t_e}^{t} q_o(\zeta)d\zeta = Q_o(t) - Q_o(t_e) = Q_o - Q_e$$

or alternatively, by substituting for θ_e from (2.22)

$$\rho_b c_b k_b(T_s - T_b)^2 = \left(\frac{\alpha}{1+\alpha}\right)^2 (Q_o - Q_e)q_o + \rho_b c_b k_b(T_a - T_b)^2\left(\frac{q_o}{q_e}\right) \tag{2.25a}$$

which may be used to solve for the ablation surface temperature T_s during the post-ablation period. Similarly, elimimating $(T_s - T_b)$ from equations (2.23) and (2.24), the thermal thickness θ for $t > t_e$ is given by

$$\theta(t > t_e) = \left[\frac{(Q_o - Q_e)}{q_o} + \left(\frac{1+\alpha}{\alpha}\right)^2 \frac{\rho_b c_b k_b(T_a - T_b)^2}{q_o q_e}\right]^{\frac{1}{2}}\left(\frac{k_b}{\rho_b c_b}\right)^{\frac{1}{2}} \tag{2.26}$$

and the surface temperature of the outer structure is again given by equation (2.13) i.e.,

$$T_w = \left[\frac{q_o(t)}{(1+\alpha)\sigma\epsilon}\right]^{\frac{1}{4}} \tag{2.27}$$

or, in dimensionless form,

$$\frac{T_w}{T^*} = \left[\frac{q_o(t)}{(1+\alpha)q_r^*}\right]^{\frac{1}{4}} \tag{2.27a}$$

Thus, the history of outer structure temperature, T_w, the ablation surface temperature, T_s, the ablation rate, and thermal penetration thickness into the ablator may be determined in terms of the material thermal properties and the imposed heating rate $q_o(t)$.

3.0 Non-Dimensional Analysis

The numerical solution of the governing equations introduced in the previous section is simplified by reducing them to non-dimensional form: Hence, it is convenient to characterize the heating rate history $q_o(t)$ in the form

$$q_o(t) = q_m F(t/t_m) \tag{3.1}$$

where q_m is the maximum heating rate during the flight trajectory, occurring at time t_m. Similarily the total heat input $Q_o(t)$ is expressed as

$$Q_o(t) = Q_m G(t/t_m) \tag{3.2}$$

The dimensionless total heat input function G is given by the ratio of integrals

$$G(t/t_m) = \frac{\int_o^{t/t_m} F(t/t_m)d(t/t_m)}{\int_o^1 F(t/t_m)d(t/t_m)} \tag{3.3}$$

Thus, $0 \leq F \leq 1$ and $0 \leq G \leq 1$ in the interval $t \leq t_m$. In the pre-ablation period the temperature at the ablation surface, given by equation (2.10) becomes

$$\left(\frac{T_s - T_b}{T_a - T_b}\right) = \frac{(FG)^{\frac{1}{2}}}{A^{\frac{1}{2}}} \tag{3.4}$$

where the ablation parameter introduced is defined by

$$A = \left(\frac{1+\alpha}{\alpha}\right)^2 \frac{\rho_b c_b k_b (T_a - T_b)^2}{Q_m q_m}$$

The ablation parameter is a dimensionless number associated with the ability of the ablator to conduct heat when subject to the imposed heating rate q_m. The thermal penetration thickness, equation (2.11), is written

$$\theta = \left(\frac{Q_m}{q_m}\frac{k_b}{\rho_b c_b}\right)^{\frac{1}{2}} \left(\frac{G}{F}\right)^{\frac{1}{2}} \tag{3.5}$$

and at $t = t_a$

$$\theta_a = \left[\frac{Q_m k_b}{q_m \rho_b c_b}\right]^{\frac{1}{2}} \left(\frac{G(t_a/t_m)}{F(t_a/t_m)}\right)^{\frac{1}{2}} \tag{3.6}$$

The surface temperature of the outer structure is now given by

$$\frac{T_w}{T^*} = \left[\frac{q_m}{(1+\alpha)q_r^*}\right]^{\frac{1}{4}} [F(t/tm)]^{\frac{1}{4}} \tag{3.7}$$

Thus in order to assure that $T_w < T^*$ we must have the inequality

$$F(t/tm) \leq \frac{(1+\alpha)q_r^*}{q_m} = R \tag{3.8}$$

The radiation parameter introduced, $R = (1 + \alpha)q_r^*/q_m$, is a dimensionless number associated with the ability of the outer surface to reject heat by radiation. The heating rate (and, indirectly, the time t_a) at which the ablation surface reaches the temperature T_a is also a function only of the ablation parameter A and satisfies the condition, from (2.12),

$$F(t_a/t_m)G(t_a/t_m) = A \tag{3.9}$$

If G is first expressed as a function of A, this equation may be solved to give

$$F(t_a/t_m) = f(A)$$

Thus in order to assure that $T_W < T^*$, we must have

$$f(A) \leq R \tag{3.10}$$

This important relation delineates a characteristic curve relating the ablation and radiation parameters. For a given trajectory, the range of values for these parameters is separated into two regions, one for which the shield/ablator combination is an acceptable design and another for which the combination will not protect the shield material from excessive heating. The shape of the curve given by (3.10) will generally vary for different trajectories, but the essential relation will remain, namely that the curve will separate the range of values for the ablation and radiation parameters into the two regions described above. This will be discussed in greater detail in the next section.

During the ablation period the solution depends on the parameter $\beta_a = q_a t_a/Q_a$ which is now rewritten as:

$$\beta_a = \left(\frac{q_m t_m}{Q_m}\right)\left[\frac{F(t_a/t_m)t_a/t_m}{G(t_a/t_m)}\right]$$

where $F(t_a/t_m)t_a/t_m/G(t_a/t_m) = F_a t_a/t_m/G_a$ is also a function of A. During ablation the outer surface temperature is given by equation (2.20) which may be written

$$\frac{T_w}{T^*} = \left\{ \frac{F_a}{R} \left[\frac{\theta_a}{\theta} + \left(\frac{F}{F_a} - \frac{\theta_a}{\theta} \right) \cdot \frac{L}{L + \alpha\eta H_o/(1+\alpha)} \right] \right\}^{\frac{1}{4}} \tag{3.11}$$

The condition on the heat of ablation L, equation (2.21), then becomes

$$\frac{1}{L} \geq \left\{ \left[\frac{F-R}{R-(\theta_a/\theta)F_a} \right] \frac{1}{\alpha\eta H_o/(1+\alpha)} \right\}_{\max} \tag{3.12}$$

This condition assures that ablation will occur as necessary to avoid excessive temperatures at the outer surface.

The governing equations during the ablation period may be simplified by making the integral thermal thickness and mass flux non-dimensional. The dimensionless quantities are:

$$\delta(\text{Thermal thickness}) = \theta/\theta_a$$

and

$$V(\text{mass flux}) = \frac{[c_b(T_a - T_b) + L + (\frac{\alpha}{1+\alpha})\eta H_o]dm/dt}{\alpha q_o(t)/(1+\alpha)}$$

The dimensionless form of Equation (2.15) and (2.16) are derived in Appendix A. The pre-ablation computations are straight-forward once the time at which ablation begins is determined from the condition given by (3.9). The solution gives the ablator surface temperature ratio, $(T_s - T_b)/(T_a - T_b)$, the dimensionless thermal thickness, δ and the outer structure (shield) temperature ratio, T_w/T^*. During ablation the differential equation for δ is solved numerically and the shield temperature ratio and dimensionless mass flux are determined as functions of dimensionless time t/t_m.

The time at which ablation ends ($V = 0$) is found by checking the numerical solution as it is marched in time. The post-ablation computations are again straightforward and give the ablator surface temperature ratio, dimensionless thermal thickness and shield temperature ratio as functions of dimensionless time t/t_m.

The characteristic heating rate function $F(t/t_m)$ used as an example in this analysis is shown in Figure 3.1. Its shape is representative of a family of curves corresponding to an equilibrium glide re-entry trajectory.

The function $F(t/t_m)$ is computed using the hypersonic approximation to the stagnation point heating rate for a spherical surface[4].

$$q_o = 0.763 Pr^{-0.6} \left(\rho_e \mu_e^{0.5} \sqrt{\frac{dU_e}{ds}} (h_{aw} - h_w \right) \tag{3.13}$$

where Pr is the Prandtl number, μ_e and ρ_e are the viscosity and density coefficients at the boundary layer edge, dU_e/ds is the velocity gradient at the stagnation point, h_{aw} is the adiabatic wall enthalpy (equivalent to the total enthalpy, H_o as used in this paper), and h_w is the actual wall enthalpy. The velocity gradient is determined from modified Newtonian theory[5,6]

$$\frac{dU_e}{ds} = \frac{1}{r_N} \sqrt{2 \left(\frac{P_e - P_\infty}{\rho_e} \right)} \tag{3.14}$$

where r_N is the radius of curvature at the stagnation point, P_e is the stagnation point pressure, and P_∞ is the free-stream static pressure. Using the hypersonic approximation, $h_w << h_{aw}$, equation (3.13) is simplified and expressed as a function of free-stream density and velocity, both functions of time for a known trajectory. Thus, $q_o = q_o(t)$ from which the heating function $F(t/t_m)$ may be determined.

Figure 3.2 depicts the total heat input function $G(t/tm)$ which is determined by numerically intregrating (3.13). Both functions are computed from a trajectory of discrete

points and then smoothed by interpolation.

The characteristic relation between the ablation and radiation parameters is determined for this trajectory from equation (3.9) and the condition $F(t_a/t_m) = R$, from equation (3.6). This is shown in Figure 3.3. As mentioned above, values of A and R which lie above the curve characterize suitable material properties (ablator and shield) and insure that T_w will remain below the critical limit T^* during the pre-ablation period. During ablation, the ablator must also satisfy (3.11) to assure this condition for the entire trajectory.

In addition to the ablation and radiation parameter curve generated, several other quantities are governed by the value of the ablation parameter. Figure 3.4 is a characteristic curve for this example of the relation between the ablation parameter and the time at which ablation begins during the trajectory. The curve is a function of the ablation parameter and shows that the dimensionless ablation time (t_a/t_m) increases with larger values of the ablation parameter hence the onset of ablation is delayed as the ablation parameter is increased. The values of the dimensionless heat flux and total heat input at the time of ablation are also determined by the ablation parameter, although the relation is an indirect one since these values are fixed by the ablation time. The characteristic curves are shown in Figures 3.5 and 3.6.

Two other quantities indirectly dependent on the ablation parameters are the the thermal thickness when ablation begins, plotted as a parameter in dimensionless form in Figure 3.7, and the parameter β used to simplify equation (2.15) and (2.16). The parameter β is defined in equation (2.18) and is used to simplify the form of the dimensionless equations solved during the period of ablation. The distinguishing feature of the parameter β is that it does not vary very much from a value of one for any given value of the ablation parameter (Figure 3.8). This allows further simplification of the governing equations and may be used to obtain an analytical solution when a quick zero-order analysis is desired. In order to visually demonstrate the concepts discussed in this section, the governing equa-

tions derived in Section 2.0 were solved for several ablating materials including water as a standard for comparison. The results are presented and discussed in the next section.

4.0 Results and Discussion

The one-dimensional thermal analysis presented in the previous two sections led to the derivation of two coupled equations to be solved numerically for a given trajectory. In this section, the results of such a numerical simulation are presented and discussed. The thermal properties of the four ablative materials[7] used as an example are presented in Table 4A. The quantity HC is the threshold enthalpy required for vaporization and replaces the quantity $c_b(T_a - T_b)$ in equation (2.15). It is assumed that the outer shield structure is limited to $T^* = 2000K$ and has an emissivity $\epsilon = 0.8$. The efficiency factor is assumed constant at $\eta = 0.5$ for simplicity. Table 4A also includes the value of the ablation and radiation parameters for each material as well as the time at which ablation begins and the time at which ablation ends. The total mass released by the ablative material per unit area of shield to be protected is also tabulated. This is determined by numerically solving the coupled dimensional equations (2.15) and (2.16).

For comparison, the performance of each material may be compared with that of water. Water is used as a standard because it has some very favorable properties as an ablator. Its relatively high heat capacity allows a high threshold enthalpy to add to a relatively high enthalpy of vaporization. Combined with a low vaporization temperature, these properties make water an almost ideal ablator for this application. The characteristic enthalpies allow it to absorb large quantity of thermal energy without excessive mass loss, while the low vaporization temperature insure that a sufficient amount of vapor will be released for the transpiration mechanism to achieve maximum effectiveness.

The ablator surface temperature ratio for the pre-ablation and post-ablation periods is shown in Figures 4.1 and 4.2. The curves for lithium flouride lie apart from the clustering of the other three primarily because of its much greater characteristic ablation tempera-

ture T_a. It also has a greater conductivity than the other ablators and thus its ablation parameter places it in the undesirable region of the ablation/radiation parameter curve (Fig. 4.6).

Figure 4.3 is a time history of the dimensionless thermal thickness θ/θ_a. The results for teflon, polyethylene, and lithium flouride reflect monotonically increasing values, while the RTV-602 ablator actually depicts a condition in which the recession rate of the ablating surface exceeds the rate at which thermal energy is conducted into the material. This causes a net decrease in the thermal thickness during ablation (RTV-602 has the lowest conductivity). The primary reason behind this is the low energy-absorption capacity per kilogram of material. The low vaporization enthalpy results in massive ablation, releasing a large amount of gaseous products. Although this effectively protects the external shield by transpiration, the total mass loss is excessive.

The dimensionless mass flux is shown in Figure 4.4. In this case, teflon, RTV-602, and to a slightly lesser degree, polyethylene quickly reach a steady ablation state (V=1) and remain there until ablation ends. Lithium flouride does not reach a steady state and ablates only for a relatively short period of time. The reasoning behind the material's poor performance may be traced to its high vaporization temperature and mediocre energy-absorption capacity as it ablates. Despite these results, lithium flouride does maintain the outer shield at or below its maximum temperature. Total mass loss is also less than the amount of water required, but teflon and polyethelene are slightly lower. As seen in Figure 4.6 the material is borderline with regards to the characteristic ablation/radiation parameter curve. One significant feature which disqualifies lithium flouride as a good choice is that during the post-ablation period, the thermal thickness increases very rapidly (Figure 4.3), a condition which would allow and excessive amount of thermal energy to penetrate the virgin material. For a finite ablation layer, this would require a prohibitive amount of material to protect the interior of the vehicle.

The shield temperature ratio is plotted in Figure 4.5 for the materials discussed. All

four materials performed well in this respect, with RTV-602 keeping the lowest profile. As previously indicated, this is due to its low total enthalpy of ablation (HC + HL), which allows it to ablate to a higher degree than the other materials, thus demonstrating the effectiveness of the transpiration cooling effect.

Based on the approximate analysis presented, the prime candidate for an ablation material in this application should have a high absorptivity coefficient to maximize the radiation parameter for a given outer shield. A combination of thermal properties should yield an ablation parameter that will place the material as close as possible to the characteristic R-A curve. This will delay the onset of ablation while still keeping the shield temperature below T^* prior to ablation. The total enthalpy of ablation (HC+HL) should be high enough to allow the material to absorb a maximum amount of thermal energy and keep total mass loss at a minimum. Vaporization temperature should be low enough so that a sufficient amount of ablation products are released to take advantage of the transpiration mechanism. The relative importance of the various thermal properties discussed will vary with the trajectory and different materials will be suitable for some and unsuitable for others. The key, nevertheless, lies with the dimensionless parameters A and R derived in this analysis as well as constraints placed on the enthalpy of ablation for any given trajectory.

These conclusions are supported by the results of the numerical simulation presented above, which clearly favor materials with a combination of thermal properties similar to teflon or polyethylene. On the basis of this approximate analysis, these materials performed according to what was hoped, maintaining the outer shield structure at or below its maximum temperature while utilizing a minimum amount of mass per unit area protected.

Although simplified to a one-dimensional analysis, the thermal protection mechanism proposed in this paper appears to have promising applications. Besides the hypersonic trans-atmospheric vehicles assumed, other aerospace structures would benefit as well, such

as inter-planetary capsules upon return to earth, atmospheric orbital transfer vehicles, and any other applications where excessive aerothermodynamic heating is of critical concern.

The next step toward possible application of this concept is to extend the analysis to more realistic geometries and to include the coupling effects of the flowfield with the thermodynamics of ablation and conduction. Finite difference analysis to model the unsteady heat conduction taking place both in the shield and the ablator material is required to more accurately determine how far the thermal energy penetrates into the virgin material. In addition, families of curves corresponding to various heating rate histories need to be categorized to determine the parameters of most importance. The characteristic relations between the various parameters introduced will vary with trajectory, but it is expected that the conclusions drawn will be universally valid.

5.0 Conclusions

A new method of thermal protection for a trans-atmospheric vehicle subject to high heating rates has been presented. By placing an ablating material behind a fixed-shape porous shield, the effectiveness of transpiration cooling may be achieved with the simplicity of a passive means of thermal protection. The simplified one-dimensional analysis treated above applies only in stagnation point regions but may be extended to include more complete geometries. Non-dimensional forms of the governing equations has led to the derivation of the controlling ablation and radiation parameters. These parameters are characteristic of the thermal properties of the ablation and shield materials for a given heating rate history and determine their potential to protect the surface from extreme temperatures during the pre-ablation period. In addition, the ablating material is required to absorb a sufficient amount of thermal energy (characterized by the heat of ablation or vaporization) if the outer shield temperature is to be kept below a specified maximum during periods of extreme heating when ablation takes place. It was also found that a relatively low vaporization temperature is favorable in order to allow the release of gaseous products and take maximum advantage of the transpiration mechanism.

A non-dimensional numerical simulation was performed using four typical ablator materials and trajectory corresponding to an equilibrium-glide re-entry into earth's atmosphere. The results indicate that ablation materials with thermal properties similar to teflon meet the criteria necessary for a successful application of this method based on the one-dimensional approximation. The use of this simplified approach indicates that the method has application potential; however the simple model presented requires further refinement to more accurately simulate unsteady conduction processes. Ultimately, detailed computational results should couple the external flowfield with the internal thermodynamics. Experimental verification is also desired prior to prototype implementation of the ablation/transpiration method of thermal protection.

References

1. Roberts, L., "An Approximate Analysis of Unsteady Vaporization Near the Stagnation Point of Blunt Bodies"; NASA TM D-41, 19059.

2. Roberts, L., "A Theoretical Study of Stagnation Point Ablation", NACA TN 4392, 1958.

3. Roberts, L., "Mass Transfer Cooling Near the Stagnation Point", NACA TN 4391, 1958.

4. van Driest, E. R., "The Problem of Aerodynamic Heating", Aeronautical Engineering Review, October 1956, pp. 26-41.

5. Tauber, M. E., Menees, G. P., and Adelman, H. G., "Aerothermodynamics of Transatmospheric Vehicles", Journal of Aircraft, vol. 24, no. 9, September 1987, pp. 594-602.

6. Tauber, M. E., "A Review of High-Speed, Convective Heat-Transfer Computation Methods", NASA Technical Paper 2914, unpublished advance copy.

7. Childs, W. H., "Thermophysical Properties of Selected Space Related Materials", The Aerospace Corp, Aerospace Report No. TOR-001 (6435-02)-1, February 1981.

7.0 Appendix A

During ablation equations (2.15) and (2.16) of Section 2.2 must be solved to give the mass flow rate, dm/dt, and integral thermal thickness, θ. The equations are

$$\frac{\alpha}{1+\alpha}q_o(t) = \left[c_b(T_a - T_b) + L + \frac{\alpha}{1+\alpha}\eta H_o\right]\frac{dm}{dt} + \rho_b c_b(T_a - T_b)\frac{d\theta}{dt} \qquad (A.1)$$

and

$$\frac{\alpha}{1+\alpha}q_o(t) = \left[L + \frac{\alpha}{1+\alpha}\eta H_o\right]\frac{dm}{dt} + \frac{k_b(T_a - T_b)}{\theta} \qquad (A.2)$$

These are reduced to non-dimensional form by introducing the dimensionless variables τ, δ, V and ϵ defined as

time

$$\tau = t/t_a - 1 \qquad (A.3)$$

thermal thickness

$$\delta = \theta/\theta_a \qquad (A.4)$$

mass flux

$$V = \frac{[c_b(T_a - T_b) + L + \left(\frac{\alpha}{1+\alpha}\right)\eta H_o]dm/dt}{\left(\frac{\alpha}{1+\alpha}\right)q_o(t)} \qquad (A.5)$$

and the parameter

$$\epsilon = \frac{c_b(T_a - T_b)}{c_b(T_a - T_b) + L + \left(\frac{\alpha}{1+\alpha}\right)\eta H_o} \qquad (A.6)$$

Equations (A1) and (A2) become

$$V + \left(\frac{q_a}{\beta_a q_o}\right)\delta' = 1 \qquad (A.7)$$

and

$$V(1-\epsilon) + \frac{q_a}{q_o \delta} = 1 \qquad (A.8)$$

where $\delta' = d\delta/d\tau$ and the relations

$$Q_a = \rho_b c_b (T_a - T_b)\theta_a$$

$$q_a = k_b (T_a - T_b)/\theta_a$$

and

$$\beta_a = q_a t_a / Q_a$$

have been used. Eequations (A.7) and (A.8) are coupled non-linear differential equations for δ and V with all other quantities including $q_o(\tau)$, $Q_a(\tau)$, and $\epsilon(\tau)$ known. A simple approximate solution for δ and V can be found for small values of ϵ as follows:

Elimination of V from equations (A.7) and (A.8) gives

$$\delta\delta' = \frac{\beta_a}{1-\epsilon} - \left(\frac{\epsilon\beta_a}{1-\epsilon}\frac{q_o}{q_a}\right)\delta \qquad (A.9)$$

the solution for $\epsilon = 0$ is

$$\delta^2 = 1 + 2\beta_a\tau \qquad (A.10)$$

Similarly, dimensionless mass flux V is given for $\epsilon = 0$ by

$$V = 1 - \frac{q_a/q_o}{(1+2\beta_a\tau)^{-\frac{1}{2}}} \tag{A.11}$$

These may be extended to first order in ϵ by returning to equations (A.7) and (A.8). Thus, to $0(\epsilon)$, the solution is

$$\delta^2 = 1 + 2\beta_a\tau - \int_o^\tau 2\beta_a[(q_o(\zeta)/q_a)(1+2\beta_a\zeta)^{\frac{1}{2}} - 1]\epsilon(\zeta)d\zeta \tag{A.12}$$

and

$$V = 1 - \frac{(q_a/q_o)}{(1+2\beta_a)\tau^{\frac{1}{2}}} + \epsilon\left[1 - \frac{(q_a/q_o)}{(1+2\beta_a t)^{-\frac{1}{2}}}\right]$$

$$-\frac{(q_a/q_o)}{(1+2\beta_a\tau)^{\frac{3}{2}}}\beta_a\int_o^\tau[q_o(\zeta)/q_a)(1+2\beta_a\zeta)^{\frac{1}{2}} - 1]\epsilon(\zeta)d\zeta \tag{A.13}$$

The results presented in Section 4.0 of this paper were obtained by direct numerical integration of equations (A.7) and (A.8). The zero-order approximation was used to derive the relation given by the inequality (2.17) or (3.12) which imposes a condition to be satisfied by the ablating material in order to avoid excessive temperatures at the outer surface.

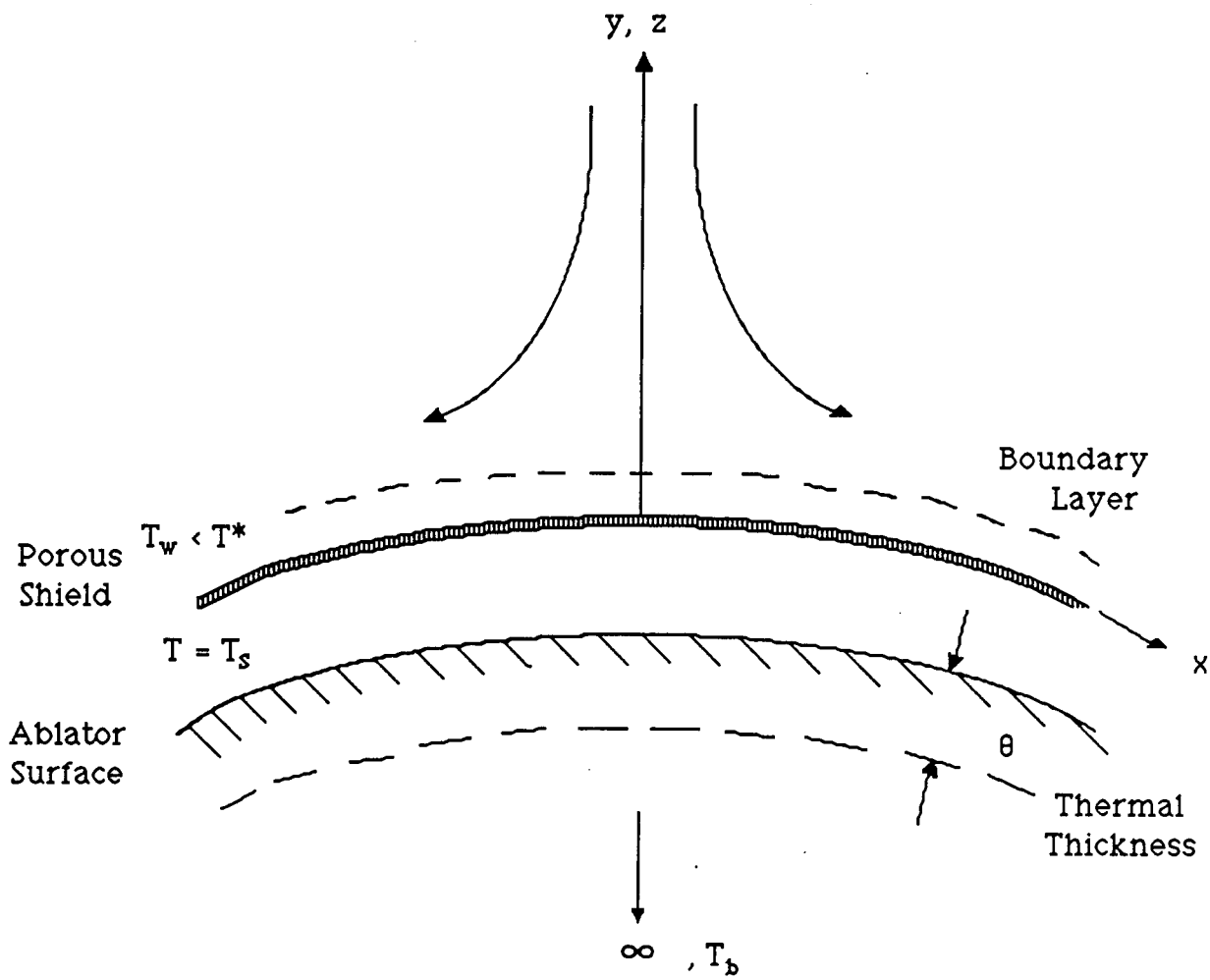

Fig. 1.1 Stagnation Point Geometry.

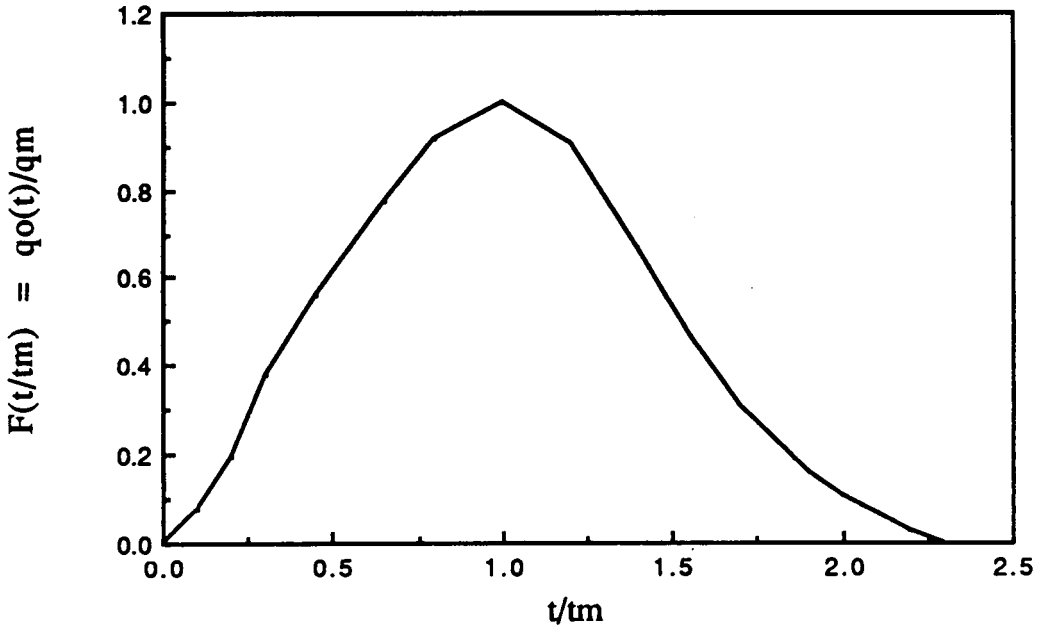

Fig. 3.1 Dimensionless Heating Rate Function.

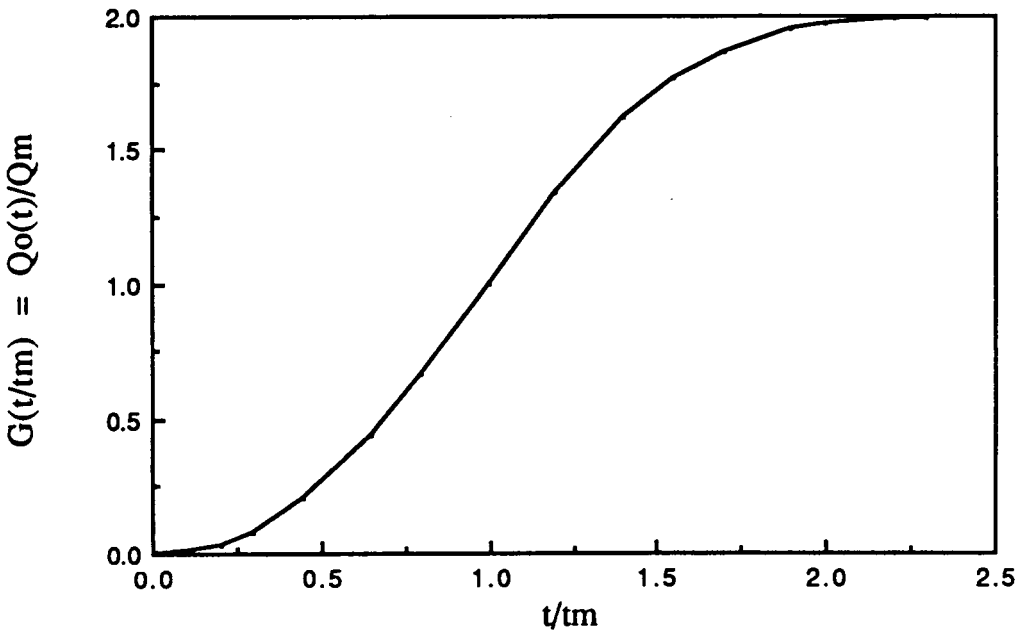

Fig. 3.2 Dimensionless Total Heat Input Function.

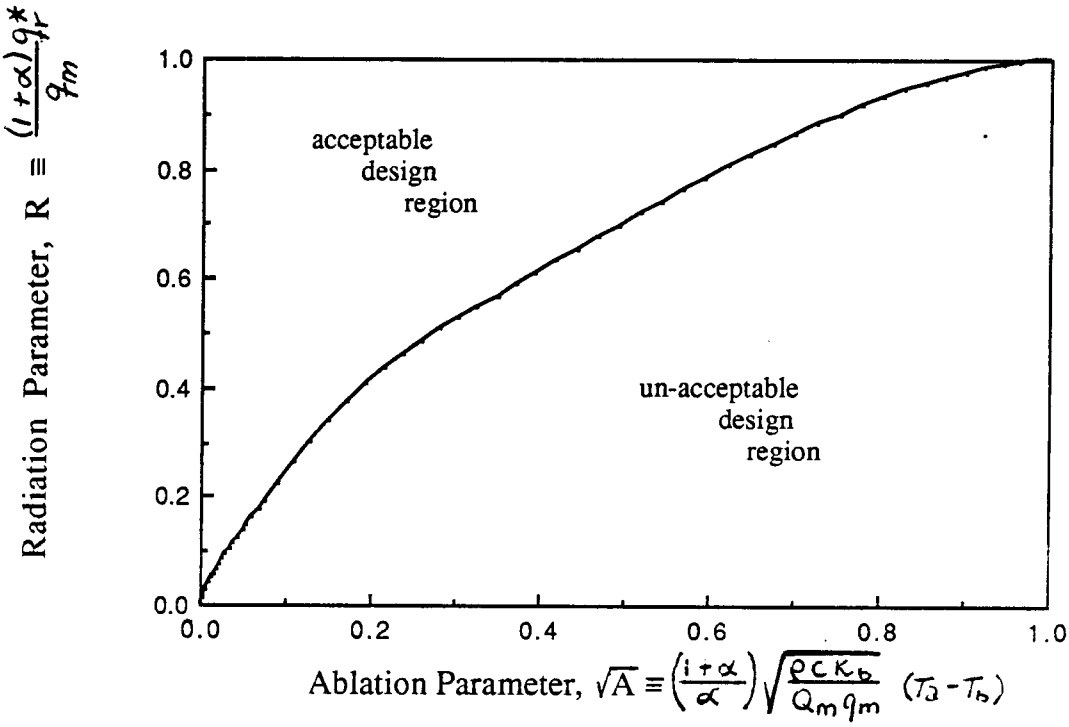

Fig. 3.3 Characteristic Curve: Radiation and Ablation Parameters.

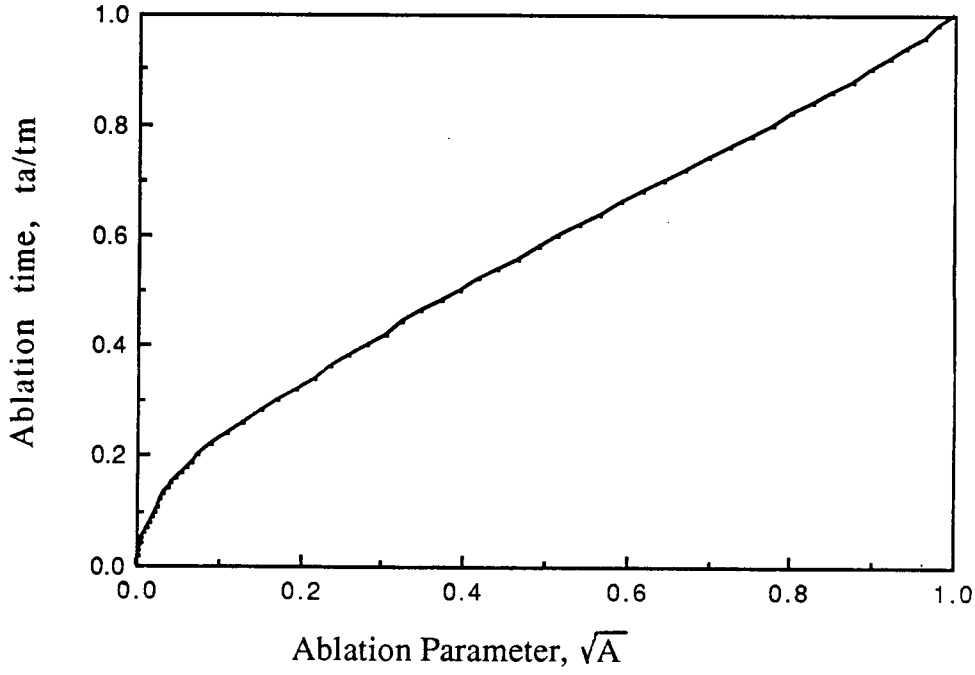

Fig. 3.4 Ablation Time vs Ablation Parameter

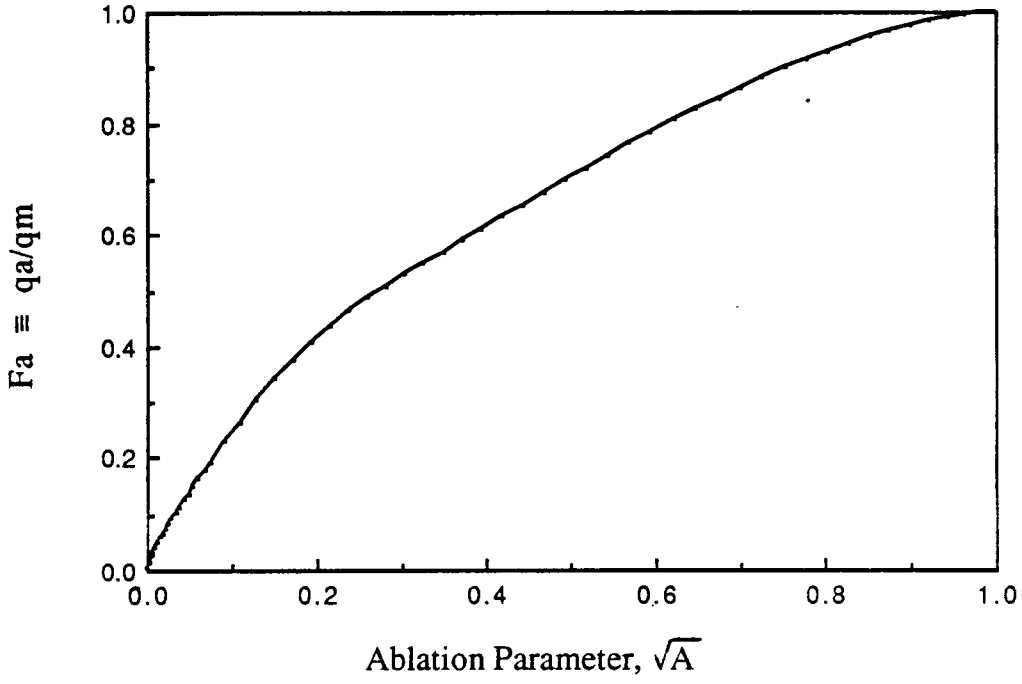

Fig. 3.5 Dimensionless Heat Flux vs $\sqrt{A}$.

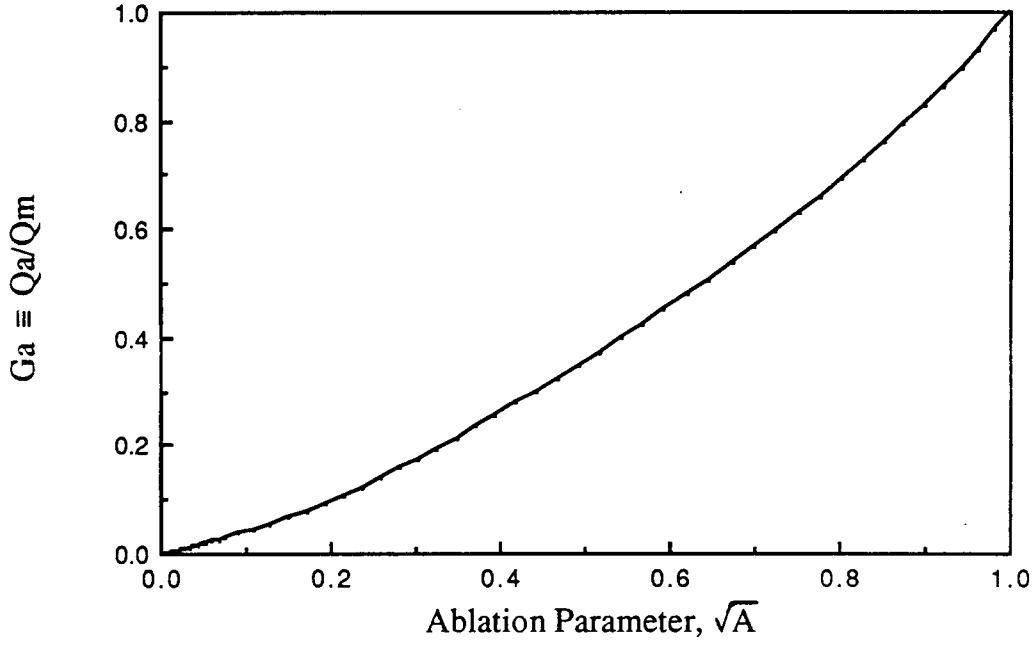

Fig. 3.6 Dimensionless Total Heat Input vs. $\sqrt{A}$.

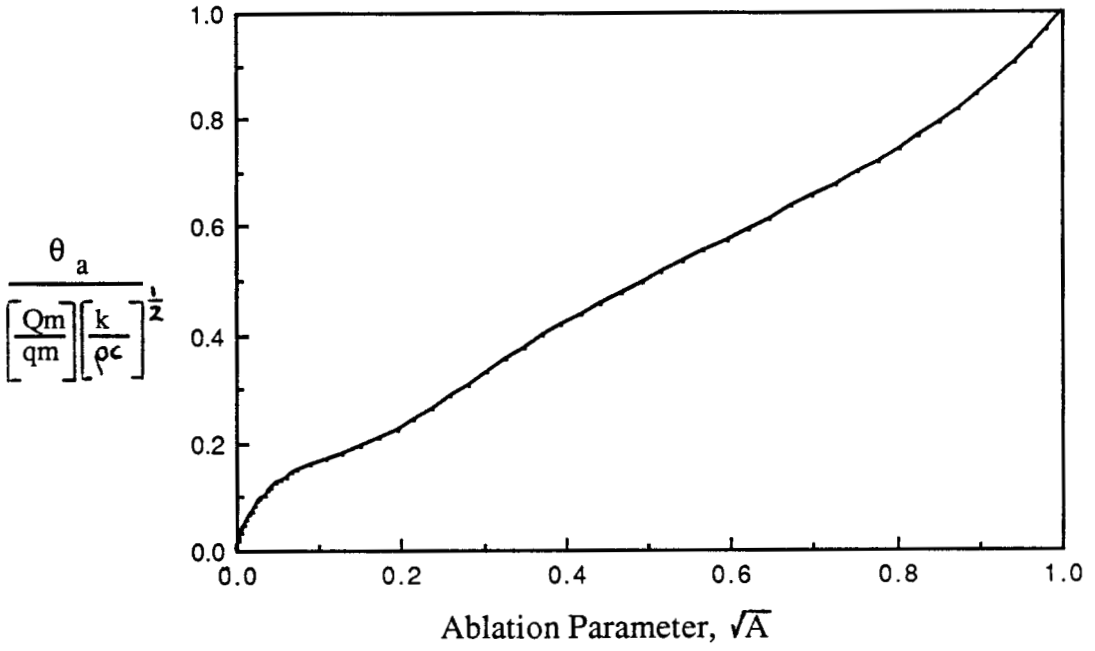

Fig. 3.7 Non-Dim. Thermal Thicknesss vs $\sqrt{A}$.

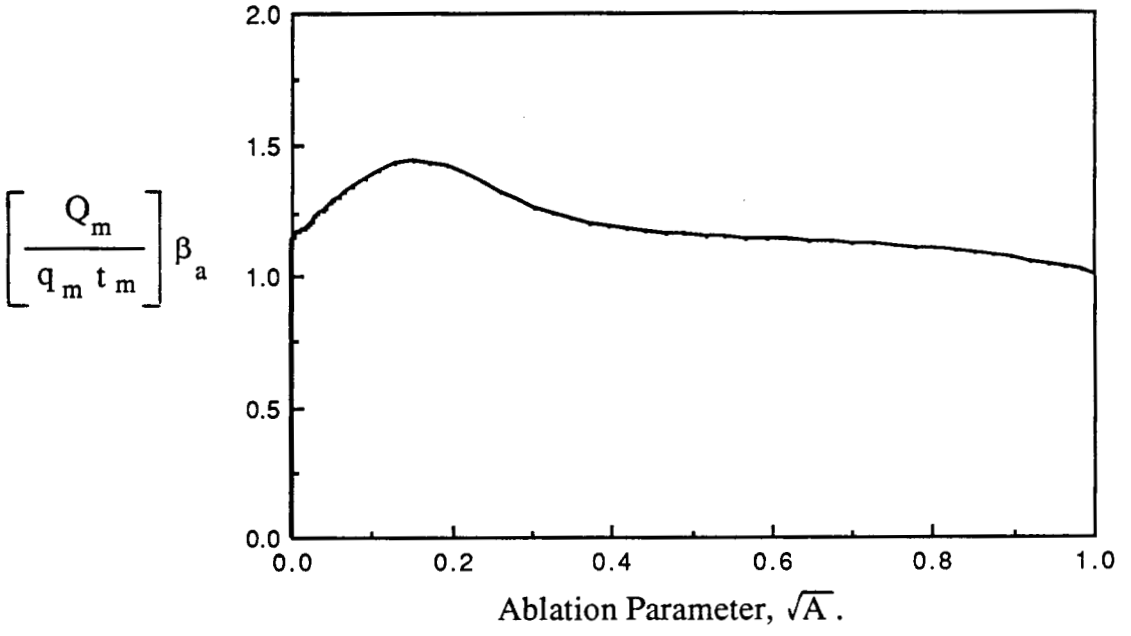

Fig. 3.8 Beta Parameter vs $\sqrt{A}$.

Table 4A : Thermal Properties of Four Ablators and Water

Material:	Teflon	Polyeth.	RTV-602	Lith. Flrd.	H_2O
Absorptivity	0.667	0.667	0.667	0.667	0.667
Ablat. Temp. T_a (K)	813.0	608.0	707.0	1966.0	373.0
Back Temp. T_b (K)	298.0	298.0	298.0	298.0	298.0
Density (kg/m^3)	2180.0	950.0	1000.0	2640.0	1000.0
Heat Cap. (J/kg/K)	1108.5	3516.3	2593.82	2025.8	4200.0
Conduct. (W/m/K)	0.308	2.320	0.278	5.749	0.600
HC (threshold; J/kg)	4.93×10^4	8.59×10^4	8.54×10^4	3.83×10^5	3.15×10^5
HL (ablation; J/kg)	6.56×10^6	4.65×10^6	4.06×10^4	7.74×10^5	2.26×10^6
ABL. Parameter, **A**	0.000282	0.00106	0.000172	0.122	2.03×10^{-5}
RAD. Parameter, **R**	0.5143	0.5143	0.5143	0.5143	0.5143
t_a (sec)	84.9	127.5	72.9	460.5	37.11
t_e (sec) *	2279.2	2259.6	2261.0	1892.0	2282.4
Mass Req'd (kg/m^2)	120.9	146.4	418.7	169.0	210.1

* Total time for heat pulse is approximately 2300 seconds.

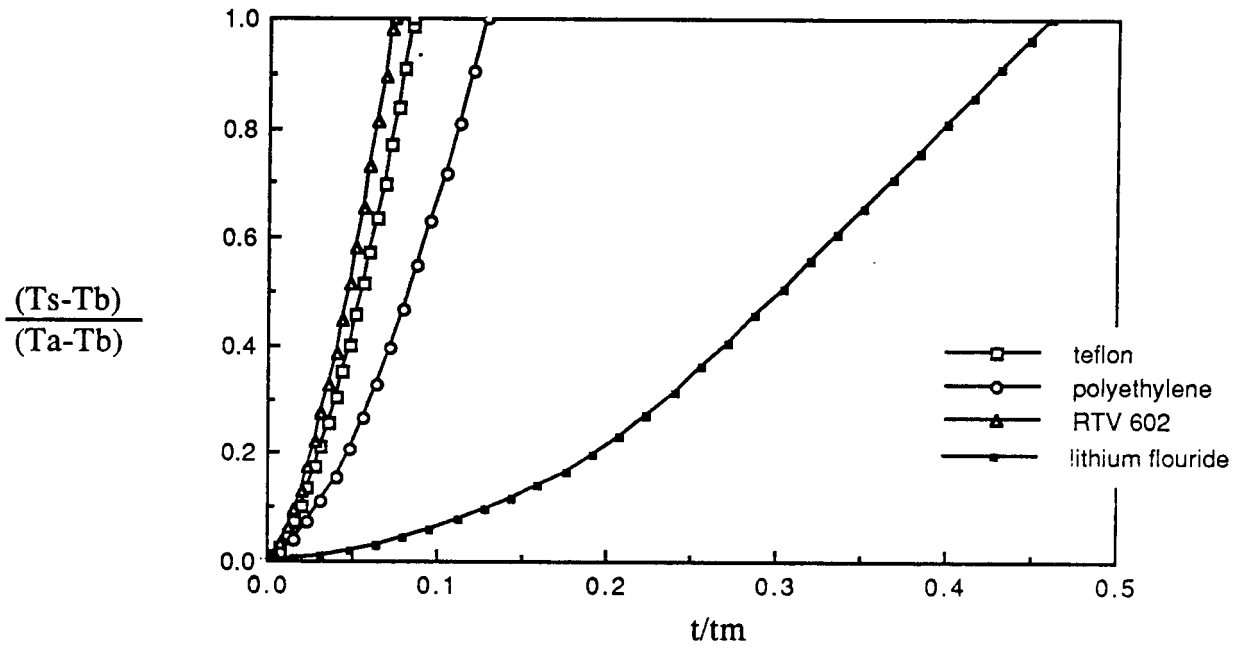

Fig. 4.1 Ablator Surface Temperature Ratio (Pre-Ablation).

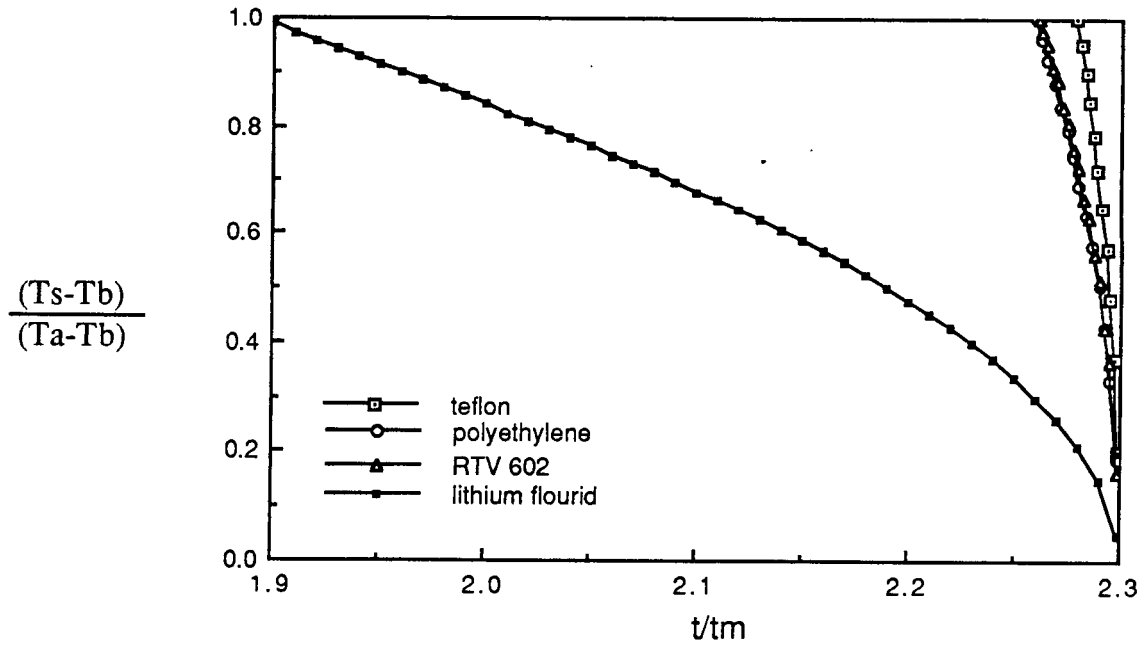

Fig. 4.2 Ablator Surface Temperature Ratio (Post-Ablation).

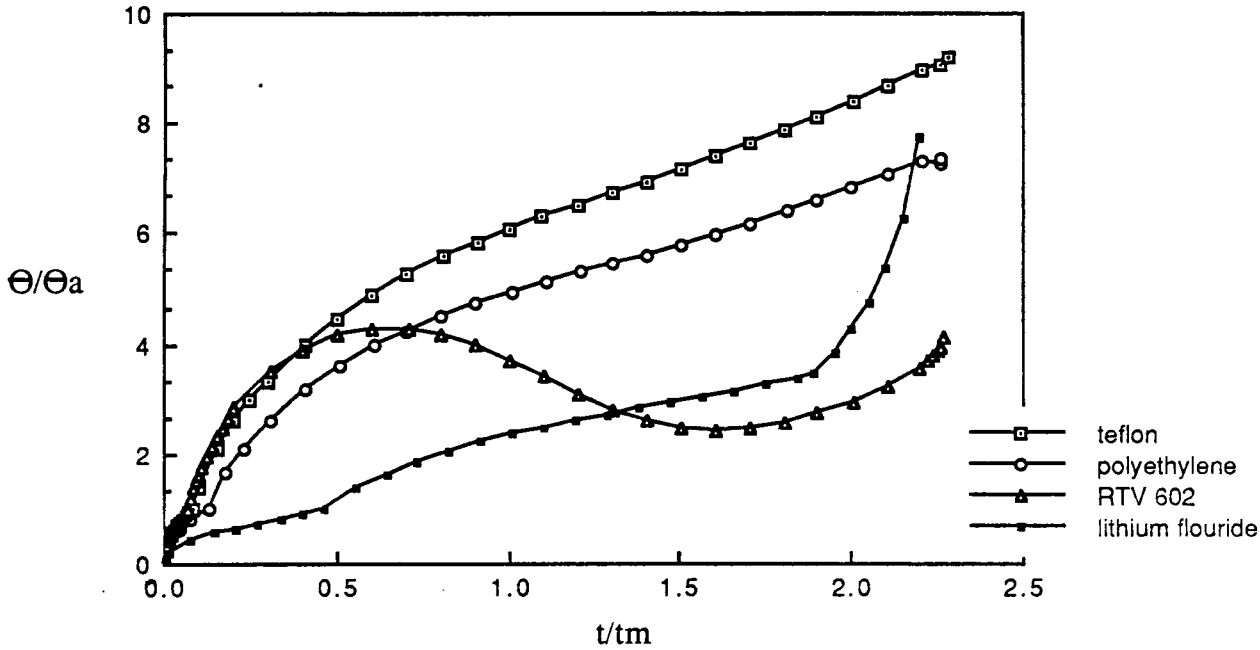

Fig. 4.3 Dimensionless Thermal Thickness.

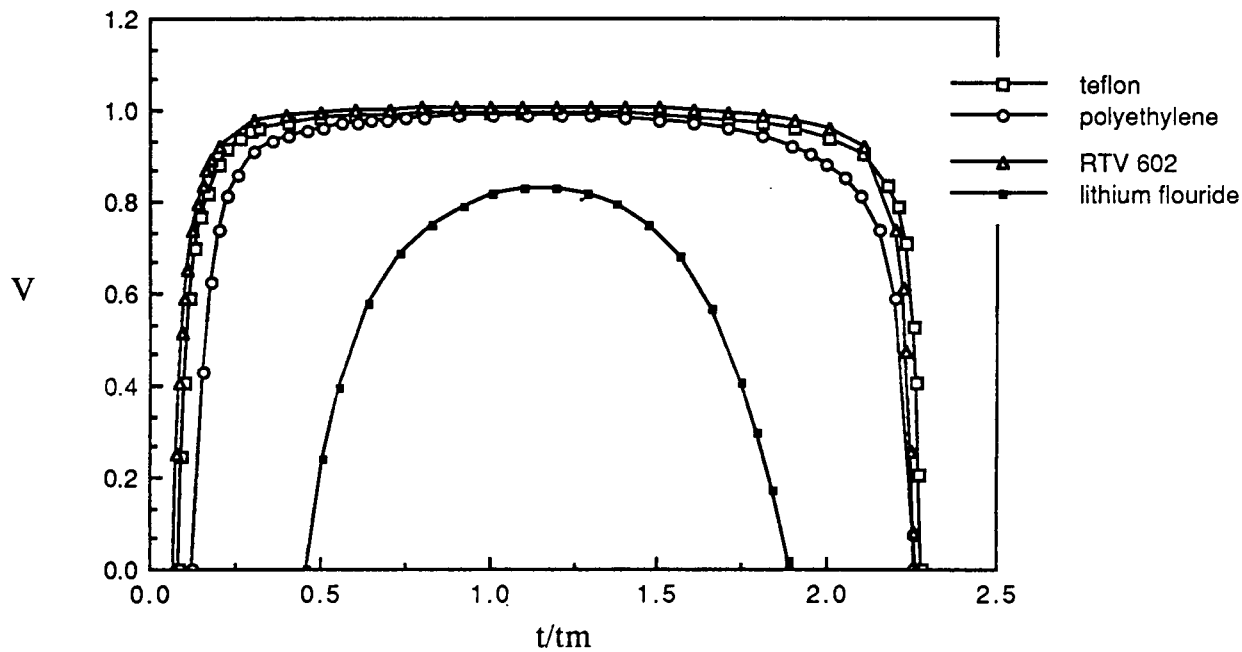

Fig. 4.4 Dimensionless Mass Flux.

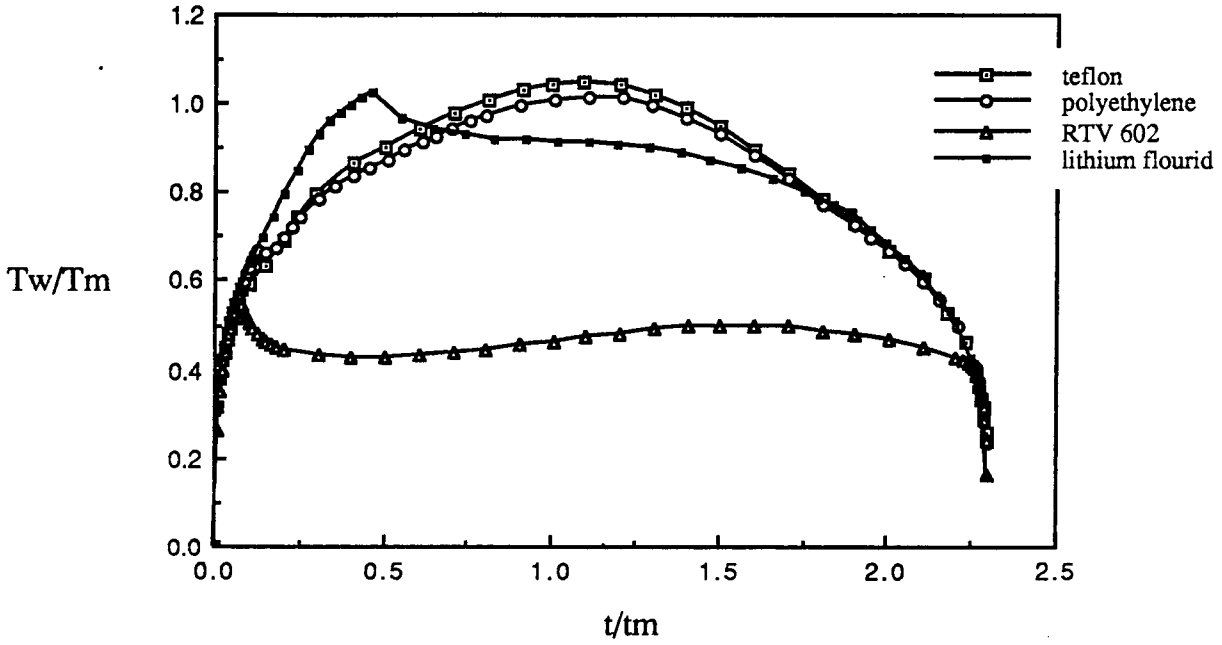

Fig. 4.5 Shield Temperature Ratio.

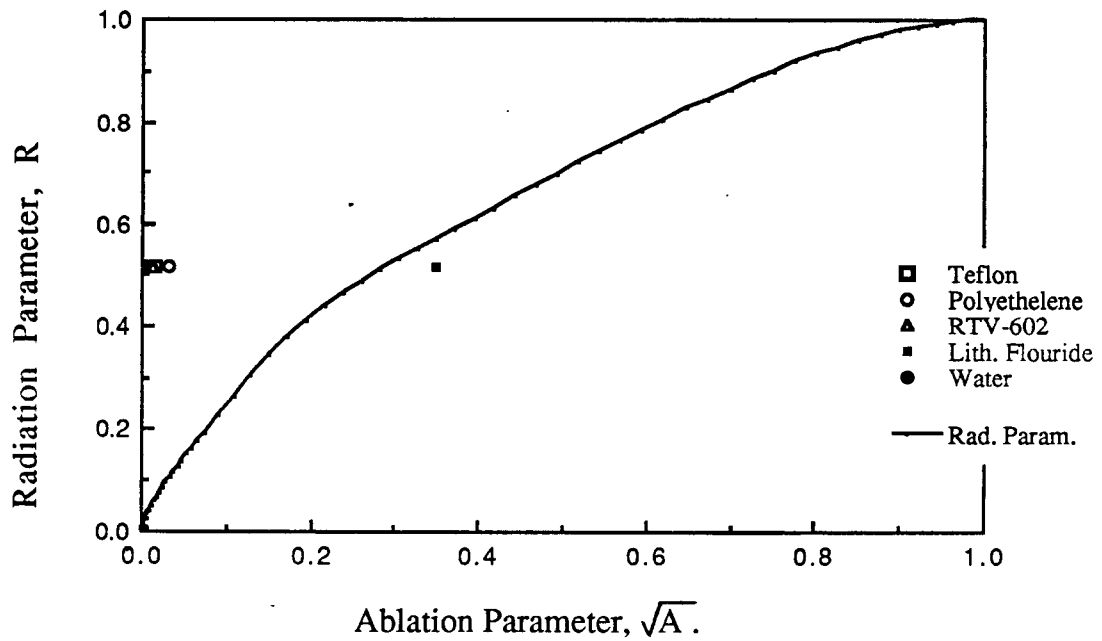

Fig. 4.6 Characteristic Parameter Curve with Four Ablators.